Chapter 3 Experimental study and optimization of OPLLs

In Chapter 2 I have presented the theory of OPLL and identified critical issues for OPLLs using SCLs. In this chapter I will present the detailed experimental study of OPLLs constructed using different commercial SCLs. I first start the chapter with the measurement of the current-frequency modulation (FM) response of SCLs. Once the FM response is known, one can include it into the open loop transfer function and model the performance of the OPLL. In Section 3.2 I will describe the experimental setup of OPLLs in details and the measurement results, in particular the spectrum of the beat signal between the master laser and the locked slave laser, from which the residual differential phase error can be characterized. In the last Section 3.3, I will discuss the use of various compensation filters and circuits to improve the acquisition range, the holding range, and the residual differential phase error.

3.1 Measurement of the FM response

In Chapter 2 I pointed out that the characteristic phase reversal of the FM response of the single-section SCLs presents the main constraint on the bandwidth of the OPLLs. Given the limited loop bandwidth, the slave laser can be locked to the master laser with reasonable locking quality only if the summed linewidth of the master laser and the slave laser is much smaller than the π phase lag frequency f_π,. The linewidth of typical SCLs lies between ~100kHz and ~10MHz and f_π is usually in the same frequency range. Thus the preliminary characterization of the linewidth and the FM response of the laser is necessary before implementing the OPLL.

The summed linewidth can be measured using a heterodyne mixing method. The signals of the master laser and the slave laser are first mixed at a high speed photodetector. An RF spectrum analyzer is then used to measure the linewidth of the photocurrent,

which is exactly the summed linewidth of the lasers. The FM response measurement, however, is more complicated and will be introduced in the following section.

3.1.1 Analysis of the FM response measurement system

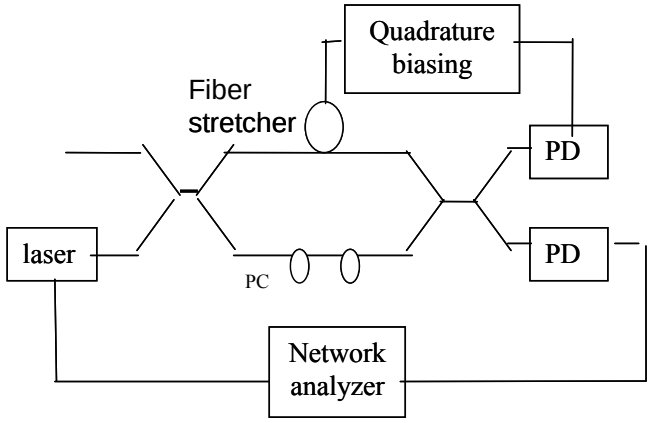

Fig. 3.1 Schematic diagram of a FM response measurement setup

The FM response of a laser can be measured with a network analyzer and an optical frequency discriminator[38]. Fig. 3.1 displays the schematic diagram of a typical FM response measurement setup. The network analyzer drives the laser with a modulation signal. The frequency of the laser is modulated and the frequency discriminator converts the frequency modulation into an intensity modulation, which is detected using a photodetector. The output of the photodetector is then fed back into the network analyzer to measure the amplitude and phase of the FM response of the laser[38].

The optical electric field fed into the frequency discriminator can be described by

$$E(t) = \sqrt{P(t)}e^{j(\omega_o t + \phi(t))} \tag{3.35}$$

where *P(t)* is the optical power, $\omega_0 = 2\pi f_0$ is the average angular frequency, and $\phi(t)$ is the optical phase. In a network analysis measurement, the laser is stimulated at a modulation frequency and its response (both amplitude and phase) is measured at the

same frequency. When the network analyzer applies a voltage modulation signal $\mathrm{Re}\left\{\tilde{V}_m e^{j\omega_m t}\right\}$ at the frequency $\omega_m = 2\pi f_m$ to the laser, the optical power is given by

$$P(t) = \mathrm{Re}\left\{P_0\left[1+\tilde{m}e^{j\omega_m t}\right]\right\} \tag{3.36}$$

where $\tilde{m}$ is a complex variable representing the intensity modulation factor. In general $\tilde{m}$ is a function of the modulation frequency.

Meanwhile the optical phase is also modulated as

$$\phi(t) = \mathrm{Re}\left\{\tilde{\phi}_m e^{j\omega_m t}\right\} \tag{3.37}$$

where $\tilde{\phi}_m$ is the complex phase modulation factor. The frequency modulation can be deduced from the phase modulation by taking the derivative of Eq. (3.37)

$$\upsilon(t) = \frac{1}{2\pi}\frac{d\phi}{dt} = \mathrm{Re}\left\{\tilde{\upsilon}_m e^{j\omega_m t}\right\} \tag{3.38}$$

where $\tilde{\upsilon}_m = \tilde{\phi}_m j f_m$ represents the frequency deviation of the optical carrier at the modulation frequency f_m.

The frequency discriminator depicted in Fig. 3.1 is simply a Mach-Zehnder interferometer. The modulated optical field is split into two signals using a fiber optical coupler. One part is delayed by time τ and then combined with the other signal again using a fiber optical coupler. The photocurrent resulted from the mixed signals is given by

$$I_D(t) \propto \left|E(t)+E(t-\tau)\right|^2 \tag{3.39}$$

where I have assumed 3-dB directional couplers and matched polarization states for the recombining signals. Substituting (3.35) into (3.39), the photocurrent becomes

$$I_D(t) \propto P(t)+P(t-\tau)+2\sqrt{P(t)P(t-\tau)}\cos\left(\Delta\phi(t)+\omega_0\tau\right) \tag{3.40}$$

where $\Delta\phi(t) = \phi(t)-\phi(t-\tau)$ is the phase difference between the recombining optical signals due to the differential delay τ through the interferometer. Information on the phase or frequency deviations of the input optical signal is contained in this phase

difference term.

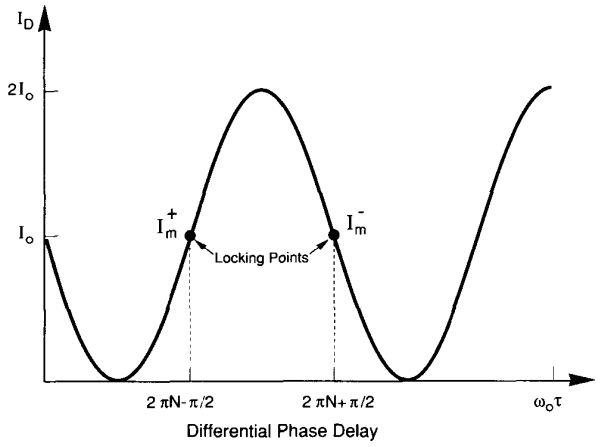

Fig. 3.2 Variation of the photocurrent at the output of a frequency discriminator as a function of the differential time delay τ without modulation.

Fig. 3.2 shows the variation of the photocurrent as a function of this differential time delay without any frequency modulation. By adjusting the differential time delay (e.g., through the use of a fiber stretcher) or the average optical frequency, the interferometer can be held in the quadrature condition (i.e., $\omega_0\tau = 2\pi N \pm \pi/2$). If both the intensity modulation and the phase modulation are small, one can plug Eqs. (3.36) and (3.38) into Eq. (3.40) and linearize it to derive the complex photocurrent

$$\tilde{I}_m(f_m) \approx I_0\left[\tilde{H}_m(f_m)\tilde{m}(f_m) \pm \tilde{H}_\upsilon(f_m)\tilde{\upsilon}_m\right] \tag{3.41}$$

where $\tilde{H}_m(f_m) = \cos(\pi f_m \tau)e^{-j\pi f_m \tau}$ is the intensity modulation transfer function and $\tilde{H}_\upsilon(f_m) = \pi\tau \sin c(\pi f_m \tau)e^{-j\pi f_m \tau}$ is the frequency modulation transfer function of the Mach-Zehnder interferometer. In our measurement, the time delay is chosen such that $f_m << 1/\tau$ which reduces $\tilde{H}_\upsilon(f_m)$ to a constant proportionality factor independent of the modulation frequency.

Eq. (3.41) shows that the measured photocurrent is a combination of both the filtered intensity modulation and frequency modulation on the optical input. One can separate the

intensity modulation and the frequency modulation responses by making two separate measurements, each biased at quadrature but on opposite slopes (see Fig. 3.2). By taking the vector subtraction of these two measurements, the intensity modulation response can be removed**.** Letting $\tilde{I}_m^+$ be the measured photocurrent at the modulation frequency while the discriminator is locked on the positive slope and $\tilde{I}_m^-$ for the negative slope (see Fig. 3.2), the FM response is obtained from Eq. (3.41) to give

$$\tilde{I}_{FM} = \tilde{I}_m^+ - \tilde{I}_m^- \approx 2I_0 \pi\tau \;\tilde{\upsilon}_m\left(f_m\right) \tag{3.42}$$

if the condition $f_m << 1/\tau$ is satisfied.

By comparing the photocurrent signal $\tilde{I}_{FM}$ to the driving voltage signal $\tilde{V}_m$, the network analyzer measures the amplitude and phase response of the whole system, including not only the FM response of the SCL, but also the response of the frequency discriminator, the photodetector, the electronics, and the delay of the optical fiber and the electric cable. This can be written down mathematically as

$$\tilde{H}'_{FM} = \frac{\tilde{I}_{FM}}{\tilde{V}_m} = \frac{\tilde{i}_m}{\tilde{V}_m} \cdot \tilde{H}_{FM}^{DFB} \cdot \tilde{H}_{\upsilon} \cdot \tilde{H}_{PD} \cdot \tilde{H}_{delay} \tag{3.43}$$

where $\tilde{H}'_{FM}$ is the measured frequency modulation response of the system, $\tilde{i}_m$ is the modulation current received by the laser, $\tilde{H}_{FM}^{DFB}$ is the current FM response of the laser, $\tilde{H}_{\upsilon}\left(f_m\right)$ is the response of the Mach Zehnder interferometer which is defined in Eq. (3.41), $\tilde{H}_{PD}$ is the response of the photodetector, and $\tilde{H}_{delay}$ represents the system delay.

To obtain $\tilde{H}_{FM}^{DFB}$, one needs to calibrate and remove the responses of all the other components. This can be done by performing an intensity modulation measurement using the same system with the shorter path of the Mach Zehnder interferometer disconnected. In this case the frequency discriminator acts as a fixed delay line. The measured intensity

modulation of the system can be described by

$$\tilde{H}'_{AM} = \frac{\tilde{I}_{AM}}{\tilde{V}_m} = \frac{\tilde{i}_m}{\tilde{V}_m} \cdot \tilde{H}_{AM} \cdot \tilde{H}_{PD} \cdot \tilde{H}_{delay} \tag{3.44}$$

where $\tilde{H}_{AM}$ accounts for the laser's intensity modulation response. The other variables are the same as those defined in Eq. (3.43). Dividing Eq. (3.43) by Eq. (3.44) one obtains the FM response of the laser

$$\tilde{H}_{FM}^{DFB} = \frac{\tilde{H}'_{FM}}{\tilde{H}'_{AM}\tilde{H}_{\upsilon}} \tilde{H}_{AM} \tag{3.45}$$

The measurement of the FM response is therefore calibrated by taking the ratio of the two measurements. The responses of the circuit, the delay, and the photodetector are automatically accounted for. For a modulation frequency much smaller than the relaxation resonance frequency of the laser, I can assume that the intensity modulation response of the laser $\tilde{H}_{AM}$ is a constant. The response of the frequency discriminator is also a constant for $f_m << 1/\tau$. Eq. (3.45) then reduces to

$$\tilde{H}_{FM}^{DFB} \sim \tilde{H}'_{FM} / \tilde{H}'_{AM} \tag{3.46}$$

Finally, the DC FM sensitivity can be obtained by changing the DC current and measuring the frequency shift.

3.1.2 Experimental measurement

To measure the FM response I constructed a FM response measurement setup similar to the one shown in Fig. 3.1. In the setup I use an Agilent 4395A network analyzer to drive the laser and measure the modulation response. The frequency range of the network analyzer is from 10Hz to 500MHz, which covers the typical thermal crossover frequency of SCLs. The photodetector I use is a New Focus 1544-B high speed photodetector. The frequency discriminator is made of two 3dB fiber couplers. The total length of the frequency discriminator (the longer path) is 1.7m and the differential delay length is

20cm which translates to the delay time $\tau \sim 1ns$. Typically the FM measurement is performed in the range of 1kHz to 50MHz, which satisfies the condition $f_m << 1/\tau$. In the measurement, the Mach Zehnder interferometer is not actively biased at its quadrature point. Thus the method described by Eq. (3.42) can not be directly used here. However, the high FM sensitivity of the SCLs combined with the high sensitivity of the frequency discriminator (proportional to the differential delay $\tau \sim 1ns$), result in the second term in Eq. (3.41) arising from the frequency modulation being typically 20dB higher than the first term arising from the intensity modulation. Therefore the intensity modulation in Eq. (3.41) can be ignored.

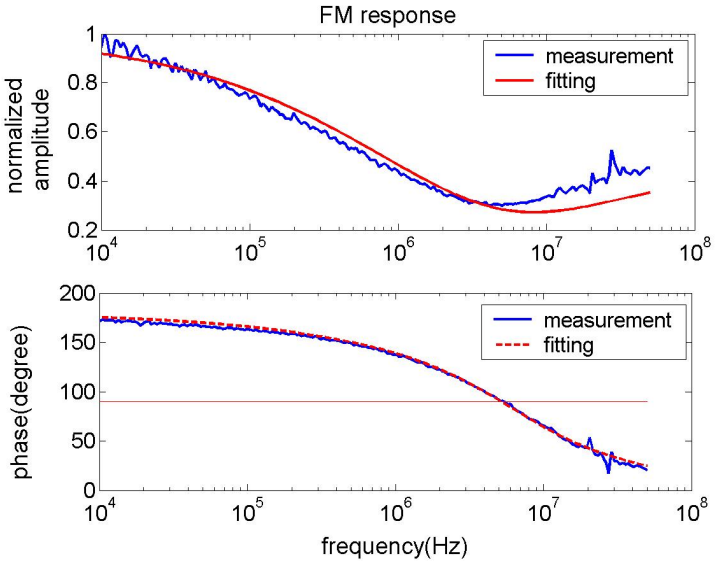

Fig. 3.3 Measurement (blue line) and theoretical fitting (red line) of the FM response of a JDSU DFB laser. The fitting parameters are: $b = 1.98$ and $f_c = 1.6MHz$.

I first measured the FM response of a JDSU CQF935/908 DFB laser. The laser is driven with an ILX low noise battery diode driver and the temperature is stabilized with an ILX TEC controller. The bias current is 400mA and the output power is 16dBm. By measuring the intensity modulation and the frequency modulation responses, I use Eq. (3.46) to calculate the FM response of the laser and the result is plotted in Fig. 3.3. The

blue solid line is the measured data and the red solid line is a theoretical fitting with the model described in Section 2.5.2 [23]

$$H_{FM}^{DFB}(f) = -\frac{K_0}{b}\left(\frac{b-\sqrt{jf/f_c}}{1+\sqrt{jf/f_c}}\right) \tag{3.47}$$

In obtaining Fig. 3.3 I have used the fitting parameters $b=1.98$ and $f_c=1.6MHz$. As I have discussed in Chapter 2.5.2, the amplitude of the FM response is not uniform and exhibits a characteristic dip at a few MHz. The phase of the FM response exhibits a π phase reversal starting from a few hundreds of kHz to a few tens of MHz.

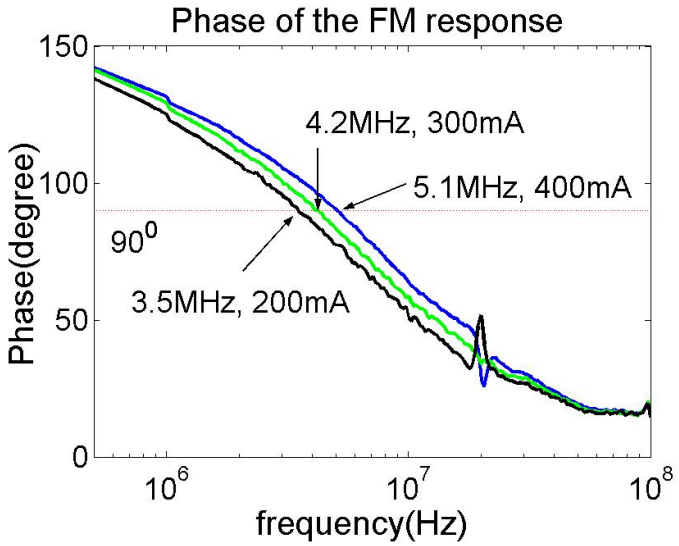

Fig. 3.4 Measured FM response of the JDSU DFB laser with different bias currents

It has been pointed out in [23] that the heat generated in the laser chip is proportional to the square of the bias current, and the small signal thermal FM strength is proportional to the bias current. According to the definition of the parameter *b* following Eq. (2.34), higher bias currents result in a stronger thermal FM contribution, which leads to a larger value of *b* and a higher thermal crossover frequency, as shown in Fig. 2.10. To confirm this I further measured the FM response of the JDSU DFB laser with bias currents of 200mA, 300mA and 400mA, respectively. The results are plotted in Fig. 3.4. As can be seen, the phase reversal of the FM response is indeed shifted to higher frequency with

higher bias current. Specifically, the 90 degree phase lag frequencies (corresponding to the π phase lag frequency in the open loop transfer function) are, respectively, 3.5MHz, 4.2MHz and 5.1MHz.

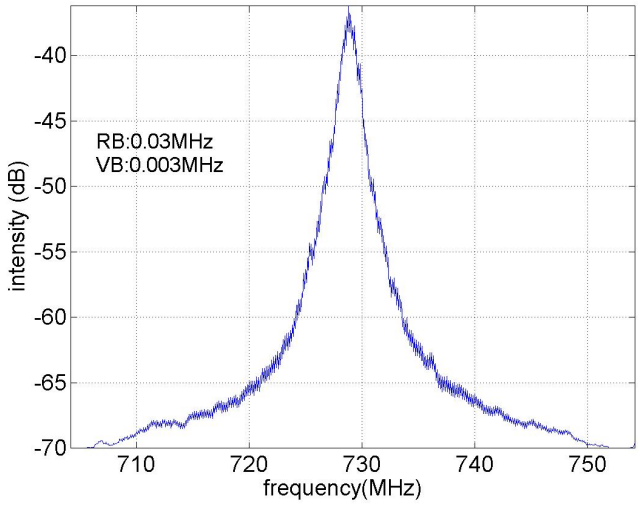

Fig. 3.5 Measured spectrum of the heterodyne beat signal between two JDSU DFB lasers

It is well known that the linewidth of a SCL is inversely proportional to the optical power[39]. Thus it is preferable to operate the laser at higher bias currents so that the loop performance can benefit from both the higher loop bandwidth (due to higher thermal crossover frequency of the FM response) and the smaller linewidth.

A straightforward method of measuring the linewidth of the laser is to heterodyne mix two lasers of similar linewidths and measure the RF beat signal on a spectrum analyzer. Fig. 3.5 gives the spectrum of the beat signal between two JDSU CQF 485 lasers measured with a HP 8565E RF Spectrum analyzer. The measured lineshape deviates from a Lorentzian shape due to frequency jitter. The summed FWHM is ~1.2MHz and the 20dB linewidth is ~ 7MHz. Since the summed 3dB linewidth is much smaller than the π phase lag frequency, $f_\pi \sim 5MHz$ determined from the non-uniform FM response, the laser can be locked.

3.2 Phase lock of different lasers

3.2.1 Phase lock of the JDSU DFB SCLs

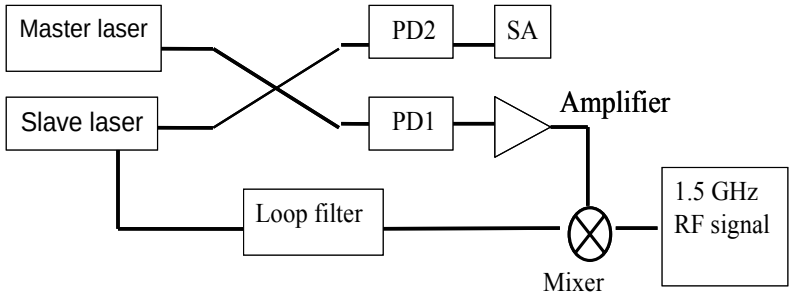

PD: photodetector SA: Spectrum analyzer

Fig. 3.6 Schematic diagram of a heterodyne OPLL.

I first built a heterodyne OPLL with the JDSU DFB laser as the slave laser and an Agilent 81640A tunable laser as the master laser. The schematic diagram of the system is plotted in Fig. 3.6. The master laser has a 3dB linewidth of about 50kHz and its output power can be adjusted from -20dBm to 3dBm. The JDSU laser is biased at 400mA and the output power is 16dBm. A 3dB 1550nm fiber optical coupler is used to combine the signals of the master laser and the slave laser. One output of the coupler is fed to the New Focus 1544B high speed photodetector, whose output is further down-converted by mixing with an offset RF signal (1.5GHz, ~15dBm) using a Minicircuits Z11-H RF mixer. The RF reference signal is produced by a HP8359A signal generator. The down-converted signal goes through a loop filter and is fed back to the slave laser to complete the negative feedback loop. The other output of the fiber coupler is fed into a HP 11982A photodetector, whose output signal is measured by an HP 8565 RF spectrum analyzer to monitor the locking status. An RF amplifier can be added following the output of the photodetector to further increase the total loop gain. With the electric gain compensation, the master laser signal can be reduced to as small as -15dBm to lock the slave laser. The fact that the loop gain can be electrically compensated enables the possibility of locking a

large number of slave lasers to one low power master laser.

The total delay time of the optical and the electric path is estimated to be about 5ns based on measuring their physical length. At the frequency of a few MHz, the phase lag due to this delay time is less than 10 degrees. Taking into account the inherent $\pi/2$ phase lag due to the integration of the current controlled oscillator, and the thermal crossover of the FM response, the π phase lag frequency f_π of the open loop transfer function should be about 5MHz. The measured acquisition range and holding range are about 9MHz.

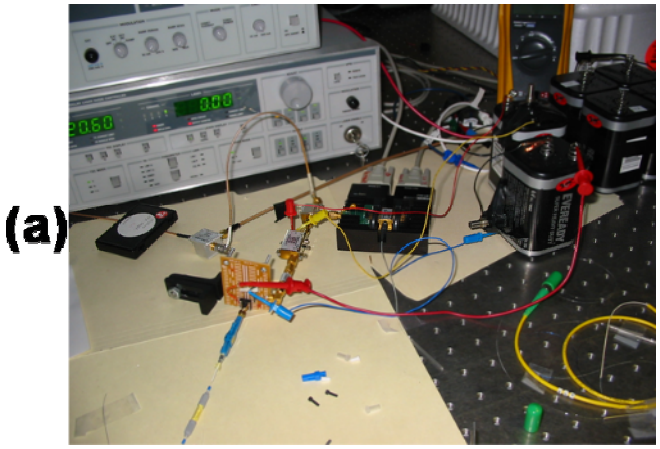

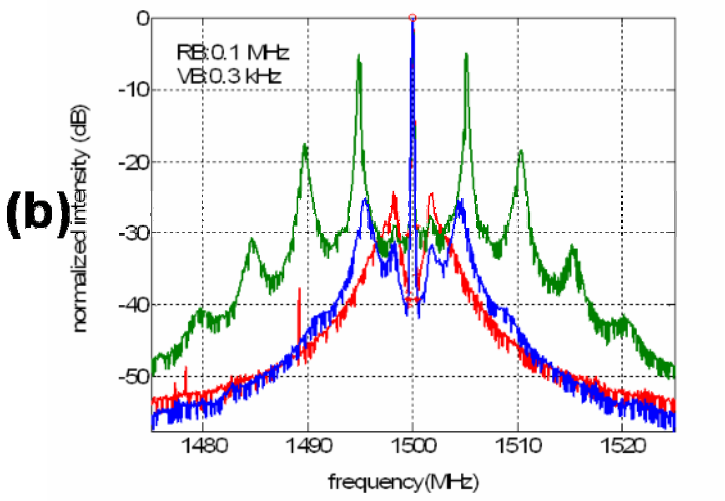

Fig. 3.7(a) A picture of the JDSU OPLL experimental setup. (b) Measured spectra of the locked beat signal of the JDSU OPLL for different loop gains.

Fig. 3.7(a) shows a picture of the actual JDSU OPLL setup. Fig. 3.7(b) shows the measured power spectra of the locked beat signal between the master laser and the slave laser for different loop gains. The red line corresponds to a low loop gain. As the loop gain is increased and the gain margin is reduced(the blue line), the frequency of the residual phase noise peak is pushed to a higher frequency. When the gain is further increased(the green line), one starts seeing the higher order side bands of the noise peak, which indicates significant ringing effect in the loop. This trend agrees with the theoretical calculation shown in Fig. 2.5. As I have pointed out in Section 2.3.3, as the gain margin approaches 0dB, the system starts oscillating at f_π. Hence the frequency difference between the central carrier and the first order noise peak in the ringing case is a good estimate of the π phase lag frequency f_π of the OPLL. In Fig. 3.7(b) f_π is about 5 MHz, which agrees with the theoretical prediction based on the measured FM response of the slave laser and the estimated loop delay.

3.2.2 Estimation of the residual differential phase error

In Section 2.5. I have pointed out the residual differential phase error is an important metric for evaluating the quality of an OPLL. Based on the measured power spectrum of the locked beat signal, one can calculate the root-mean-square (rms) differential phase error.

Assume the locked beat signal takes the form of

$$E = E_0 \cos\left(\omega_{rf} t + \phi_n\right) \tag{3.48}$$

where ω_{rf} is the frequency of the RF offset signal. When the two lasers are locked, the phase noise ϕ_n is bounded. Assuming $\phi_n << 1$, one can expand Eq. (3.48) to

$$E \approx E_0[\cos\omega_{rf} t - \sin\omega_{rf} t \cdot \phi_n] \tag{3.49}$$

The first term is a pure tone at the frequency of ω_{rf} which gives the central carrier

signal in the power spectra shown in Fig. 3.7(b). By averaging the square of the electric field over a time scale much longer than the period of the signal, one obtains the power of the signal as $P_s \sim E_0^2$. The second term in Eq. (3.49) leads to the double side noise shoulder seen in Fig. 3.7(b) when there is no significant ringing effect. Use the same argument described above, the power of the second term in Eq. (3.49) is $P_n \sim E_0^2 \overline{\phi_n}^2$, which can be calculated by integrating the double side power spectral density excluding the central carrier. From the ratio between the noise power and the carrier power one can estimate the rms differential phase error

$$\bar{\sigma} = \sqrt{\overline{\phi_n}^2} = \sqrt{P_n / P_s} \tag{3.50}$$

In Fig. 3.7(b), the rms phase error of the blue curve is about 0.32 *rad*.

3.2.3 Phase lock of the QPC MOPAs

Based on the same OPLL scheme, I also phase locked a QPC semiconductor Master-Oscillator-Power-Amplifier (MOPA) laser to the Agilent tunable laser. The MOPA is soldered on a C-mount, which is mounted on a copper block for heat dissipation. The MOPA is temperature controlled and operated with bias currents of 485 mA and 4 A, for the oscillator section and the amplifier section respectively. The wavelength of the MOPA is 1548nm and the output power is ~1W. The measured linewidth is less than 1MHz. The beam of the MOPA diverges in free space and part of the optical power is collected using a cleaved single mode fiber and then combined with the reference optical signal using a 3dB optical fiber coupler. The resulting phase error signal is injected into the oscillator section to modulate the optical frequency. Fig. 3.8(a) gives a picture of the actual setup and Fig. 3.8(b) displays the measured spectrum of the locked beat signal. The differential phase error between the slave laser and the master laser is calculated with Eq. (3.50) to be about 0.3 *rad*.

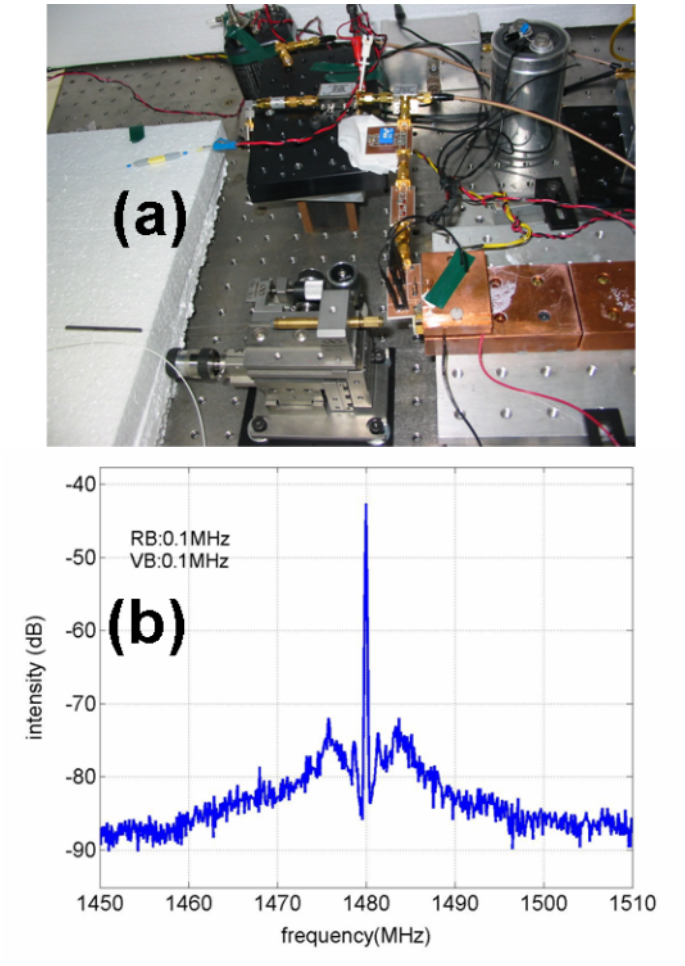

Fig. 3.8 (a) A picture of the QPC OPLL experimental setup. (b) Measured spectrum of the locked beat signal.

3.2.4 Phase lock of IPS external cavity lasers

I also phase-locked 75mW 1064nm external cavity SCLs (Innovative Photonic Solutions) with a 3 dB FWHM linewidth of 0.5 MHz. The reference laser is a spectrally stabilized NP Photonics fiber laser with a 3dB FWHM linewidth of 2.5 kHz. Fig. 3.9 gives the spectrum of the locked beat signal. A compensation filter with the lag-lead property at low frequency and the lead-lag property at frequency close to the f_π is used, and the rms differential phase error is about 0.13 *rad*. The topic of the compensation filter will be discussed in detail in the next section.

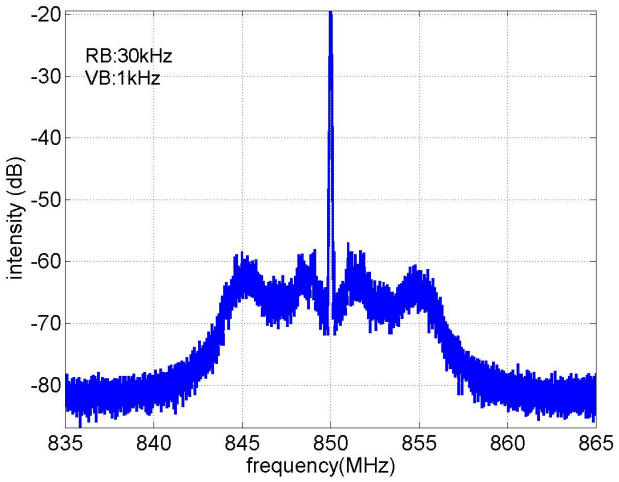

Fig. 3.9 Measured spectrum of the locked beat signal of the IPS OPLL.

3.3 Optimization with the compensation circuits

In Chapter 2 I pointed out that the loop bandwidth is limited by the non-uniform FM response of SCLs and the loop delay. This results in a number of critical issues, besides the non-negligible residual phase error. For example, the acquisition range and the holding range, which are proportional to the loop DC gain for the first-order PLL, are only a few MHz in the OPLLs I built. Upon being turned on, the frequency of the beat signal has to be manually tuned to be within ~10MHz from the frequency of the RF reference signal for the loop to acquire lock. In addition, the frequency of the SCLs jitters for tens of MHz within a few seconds, and hundreds of MHz over the long term, due to thermal fluctuations, current source noise, and acoustic noise. When the holding range is small the frequency jitter of the SCLs constantly throws the loop out of lock. All these issues can be partially solved by using certain compensation circuits. In this section I will study the use of three types of compensation circuits: the phase lead-lag filter, the lag-lead filter, and the aided-acquisition circuit.

3.3.1 Lead-lag filter to increase the phase margin

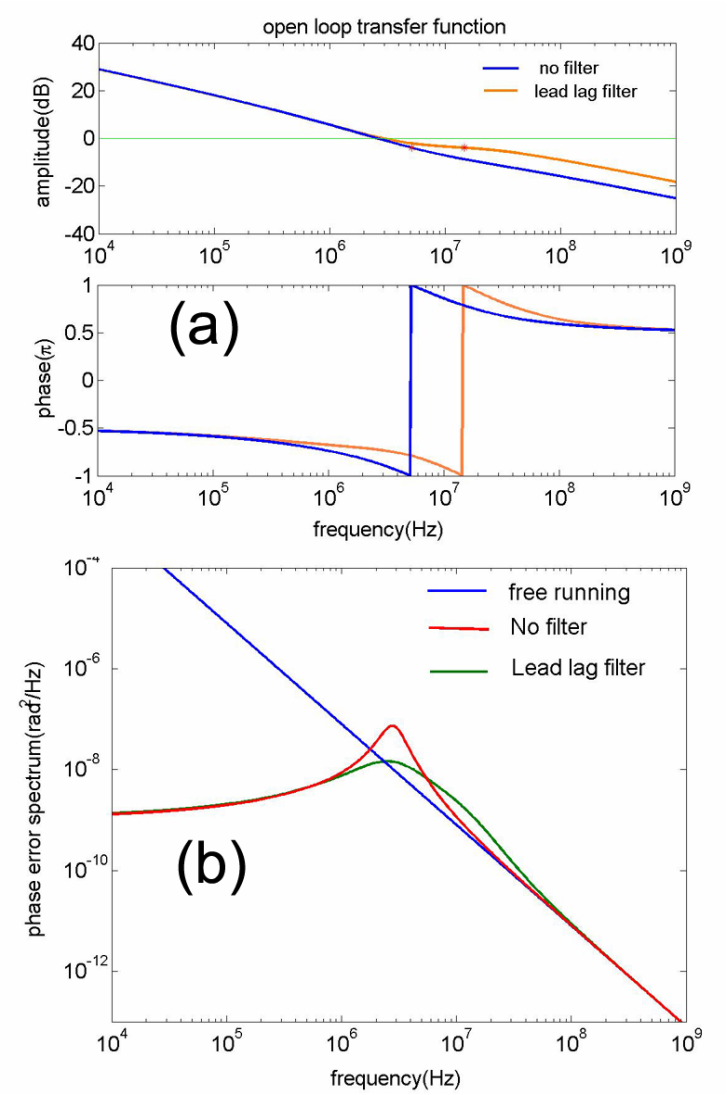

Fig. 3.10(a) Open loop transfer function of the JDSU OPLL with and without a lead-lag filter. (b). Corresponding power spectral density of the differential phase error. The FM response of the slave laser is described by Eq. (3.47) with b = 2.6, f_c = 1MHz. The transfer function of the filter is $F = (1+\tau_2 s)/(1+\tau_1 s)$ with $\tau_1 = 8ns$ and $\tau_2 = 40ns$.

As can be seen, the π phase lag frequency f_π is limited to a few MHz, due mainly to the phase lag given by the non-uniform FM response of the laser. Phase lead-lag filters can be used to increase f_π. The transfer function of a lead-lag filter is

$$F = \frac{1+\tau_2 s}{1+\tau_1 s},\ \ \tau_2 > \tau_1 \tag{3.51}$$

Eq. (3.51) can be included into the OPLL open loop transfer function to evaluate its influence. In Fig. 3.10(a) I compare the open loop transfer function with and without a lead-lag filter. In the calculation I use the FM response of the slave laser described by Eq. (3.47) and the parameters b = 2.6, f_c = 1MHz. The parameters of the lead-lag filter are $\tau_1 = 8ns$ and $\tau_2 = 40ns$. With the lead-lag filter f_π is increased from 5MHz to 14MHz. However this comes at the cost of reduced gain margin because the lead-lag filter raises the loop gain at high frequency. This can be seen in Fig. 3.10(a). The amplitudes of the blue (no filter) and the orange (with the lead-lag filter) lines are the same at low frequency. The amplitude of the orange line rises above the blue line at higher frequency. In Fig. 3.10(b) I also compare the power spectral density of the differential phase error without and with a lead-lag filter. On the diagram, the spectral peak at the frequency close to f_π is suppressed and broadened with the filter.

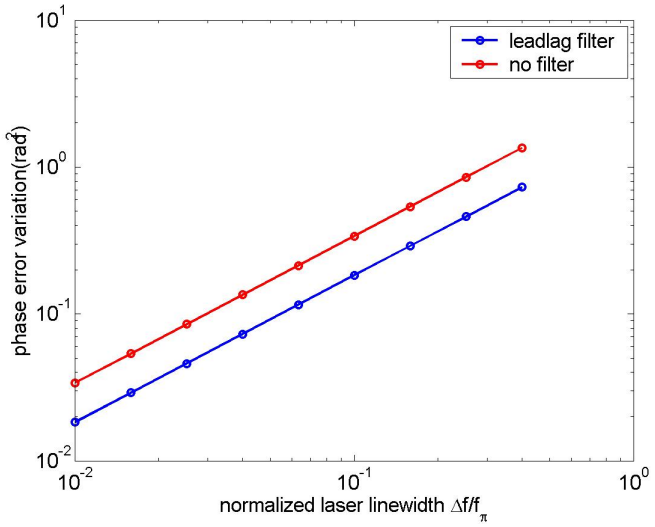

Fig. 3.11 The variance of the differential phase error as a function of the summed linewidth of the lasers Δf normalized by the π phase lag frequency f_π, with and without a lead-lag filter.

I further calculate and compare the variance of the differential phase error as a function of the normalized linewidth $\Delta f / f_\pi$ with and without a lead-lag filter. The results are plotted in Fig. 3.11. With the lead-lag filter the variance of the differential phase error can be reduced by almost a factor of 2.

Experimental demonstration

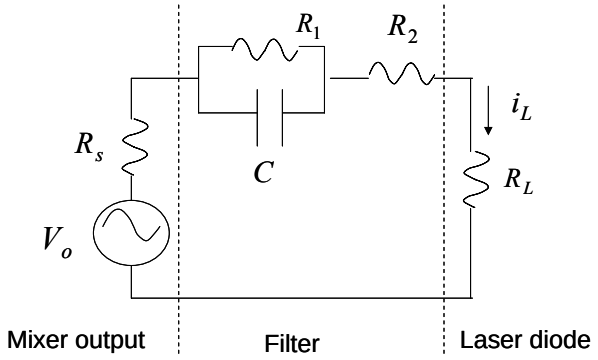

Fig. 3.12 Schematic diagram of the feedback circuit with a lead-lag filter

I have implemented a lead-lag filter in the JDSU OPLL and the circuit diagram is shown in Fig. 3.12. The mixer is modeled as a voltage source V_0 with the internal impedance R_s. The phase error voltage signal is filtered and converted to the current feedback signal i_L and sent into the laser diode R_L. A straightforward calculation leads to

$$i_L = \frac{V_o}{R_L + R_2 + R_1 + R_s} \frac{1+\tau_2 s}{1+\tau_1 s}, \tag{3.52}$$

where $\tau_1 = R_1 \left(R_L + R_s + R_2 \right) C / \left(R_L + R_s + R_1 + R_2 \right)$, $\tau_2 = R_1 C$. All the parameters are defined in Fig. 3.12.

The filter is implemented with the parameters $R_1 = 430\Omega$, $R_2 = 7.3\Omega$, and $C = 100 pF$. Impedance of the laser diode is $R_L \approx 3\Omega$ and impedance of the mixer is $R_s = 50\Omega$. Using these numbers I obtain the time constants $\tau_1 = 5.3 \times 10^{-9} s$ and

$\tau_2 = 4.3\times10^{-8} s$. With the same fitting parameters used in obtaining Fig. 3.3, one finds that the π phase lag frequency f_π is increased from 4.3 MHz to 11MHz with the filter.

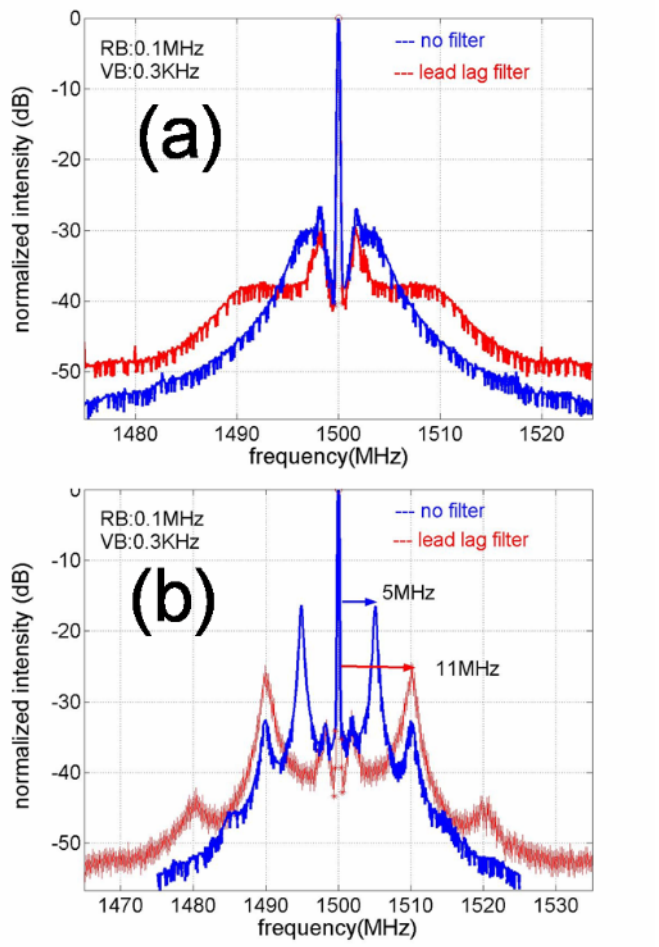

Fig. 3.13 Measured spectra of the locked beat signal of the JDSU OPLL without and with a lead-lag filter. The loop gain is increased in (b) such that the π phase lag frequency f_π can be estimated from the ringing frequency.

Fig. 3.13 is a comparison of the measured spectra of the locked beat signal with and without the lead-lag filter. In Fig. 3.13(a) one can see the noise shoulder is suppressed and broadened as predicted in Fig. 3.10(b). By integrating the double-sided noise power

spectral density, the variance of the phase noise is found to be reduced from 0.081 rad^2 to 0.053 rad^2. I further increase the loop gain until the ringing effect appears and the loop is close to oscillation, as indicated by the multiple side peaks shown in Fig. 3.13(b). The frequency difference between the central carrier and the first side peak gives a good estimate of f_π, which is increased from 5MHz to 11MHz as predicted by theory.

3.3.2 Passive lag-lead filter to increase the holding range

The frequency of SCLs strongly depends on the bias current and the temperature. E.g., the JDSU DFB laser has a current-frequency tuning sensitivity of ~500MHz/mA and a temperature-frequency tuning sensitivity of ~10GHz/C. Even with a high accuracy TEC controller and a low noise current source, I have seen that the frequency of the laser jitters by tens of MHz within a few seconds, and hundreds of MHz over tens of minutes. For external cavity SCLs, the frequency is also very sensitive to acoustic perturbation. The frequency jitter due to the current and temperature variation can throw the loop out of lock frequently, since the holding range is typically ~10MHz. In the experiment, the JDSU OPLL typically stays in lock for about 10 seconds without using a compensation filter.

In Section 2.2 I have also pointed out that the steady state differential phase error relies on the free-running frequency difference between the lasers normalized by the loop DC gain, i.e., $\Phi_{e0} = \Delta\omega / K_{dc}$. And the small signal loop gain $K'_{dc} = K_{dc}\cos\Phi_{e0}$ relates to $\Delta\omega$ through Φ_{e0}. Even when the loop stays in lock, the frequency jitter changes the steady state differential phase error Φ_{e0} and the small signal loop gain, events which should be avoided or minimized.

The frequency of SCLs can be stabilized to a very high degree by frequency locking to a stable frequency reference. The frequency reference could be a stabilized Fabry-Perot cavity[40, 41] or the absorption line of certain molecules[42]. However these solutions

require complicated systems and the advantages of SCLs, such as their small size and low cost, are lost. Also limited are the choices of molecules' absorption lines, to which the SCLs can be locked. Here I study a more attractive solution, i.e., the use of the lag-lead filter to compensate for the frequency jitter of the SCLs.

In a PLL, the acquisition range Δf_{acq} depends on the detailed shape of the open loop transfer function, and the holding range Δf_h is mainly determined by the loop DC gain $\Delta f_h = K_{dc}/2\pi$ [1]. In a practical OPLL, the loop gain is limited by the stability criterion $G_{op}(f_\pi) < 1$ and f_π is usually limited to a few MHz, due to the non-uniform FM response of SCLs and the loop delay. If one increase the loop gain only at frequencies lower than f_π and do not reduce the gain margin at f_π, the stability criterion is still maintained while the holding range Δf_h is increased. This can be achieved using a lag-lead filter. The transfer function of a lag-lead filter can be described by

$$F(s) = \frac{1+\tau_2 s}{1+\tau_1 s}, \quad \tau_1 > \tau_2 \tag{3.53}$$

Fig. 3.14(a) shows the Bode plot of a typical lag-lead filter. The filter has high gain at low frequency and reduced gain at higher frequency. In Fig. 3.14(b) I compare the open loop transfer function of the JDSU OPLL without and with a lag-lead filter. The open loop gain at low frequency, and the resulting holding range is enhanced by a factor of τ_1/τ_2. A theoretical study has demonstrated that the acquisition range can also be enhanced by approximately $\sqrt{2\tau_1/\tau_2}$ [1]. The benefit, however, comes at the cost of a reduced phase margin at the intermediate frequency($10^4 \sim 10^5 Hz$ in Fig. 3.14(b)) due to the phase lag property of the filter. Hence, care must be taken while picking the time constants τ_1 and τ_2 to maintain sufficient phase margin and avoid loop instability. In

addition, the frequency range of the phase lag induced by the filter should be kept far away from the f_π without affecting it.

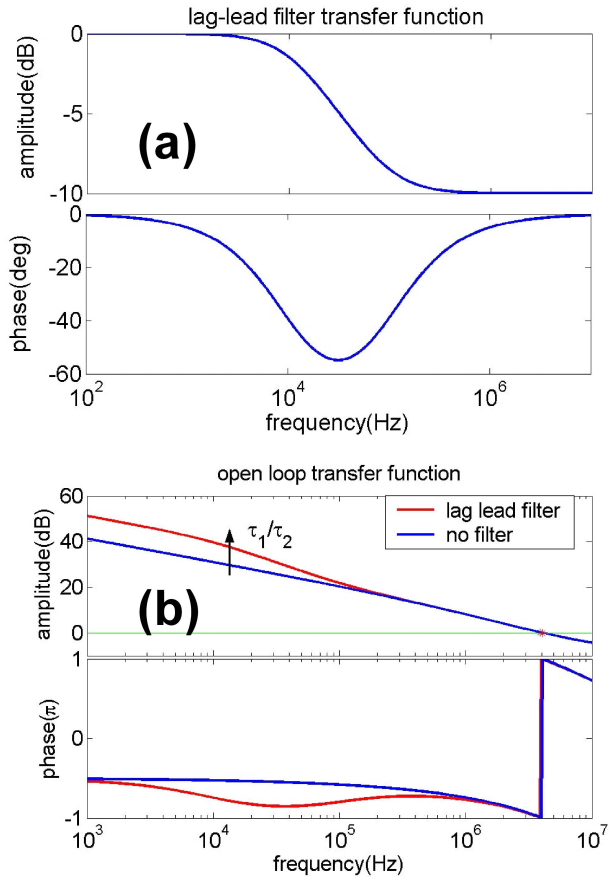

Fig. 3.14 (a) Transfer function of a lag-lead filter. (b). The open loop transfer function of the JDSU OPLL without and with a lag-lead filter. Eq. (3.47) and the parameters b = 2.6, f_c = 1MHz are used in the calculation. The transfer function of the filter is $F = (1+\tau_2 s)/(1+\tau_1 s)$ with $\tau_1 = 124\mu s$ and $\tau_2 = 6\mu s$

Experimental result

I have implemented a passive lag-lead filter illustrated in Fig. 3.15. With the parameters defined in Fig. 3.15, the feedback current is given by

$$i_L = \frac{V_o}{R_L + R_3 + R_1 + R_s}\frac{1+\tau_2 s}{1+\tau_1 s} \tag{3.54}$$

where $\tau_1 = \left[R_2 + \left(R_L + R_3 \right) \left(R_s + R_1 \right) / \left(R_L + R_3 + R_s + R \right) \right] C$ and $\tau_2 = R_2 C$. Two sets of lag-lead filter parameters were tried in the JDSU OPLL and the results are listed in table 3.1. The holding range is increased by ~6 times with filter 1 and ~16 times with filter 2. If one assumes that the frequency jitter is a random walk process, if the holding range is increased by a factor of τ_1 / τ_2, the average time required for the frequency jitter to exceed the holding range should increase by a factor of $\left(\tau_1 / \tau_2 \right)^2$. In the experiment I observed that the locking duration is increased from ~10 seconds to hours. I also implemented the lag-lead filters in the IPS OPLL and successfully increased the holding range from ~±10MHz to ±200MHz.

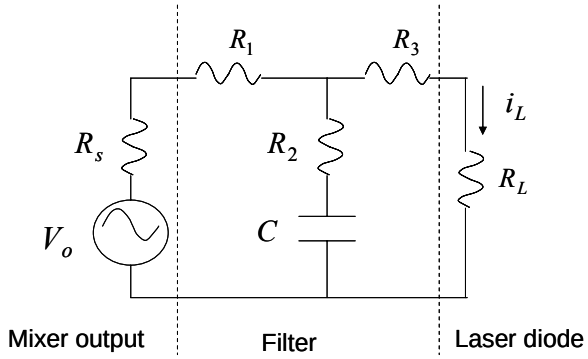

Fig. 3.15 Schematic diagram of the lag-lead filter circuit

Table 3.1 Measured single-side holding range and acquisition range of the JDSU OPLL with the lag-lead filters.

	holding range (MHz)	acquisition range (MHz)
no filter:	8 ~ 10	6 ~ 8
filter 1	50 ~ 60	~ 17
filter2	130 ~ 180	~ 30

Further increase of the holding range with the passive lag-lead filter will be

ultimately limited by the current driving capability of the RF mixer, since it is the mixer that provides the feedback current to hold the slave laser in lock. For a typical level7 mixer (e.g., the minicircuits zx05-C24), the maximum output current is about +/-2mA, which translates to a holding range of a few hundred MHz to 1GHz, depending on the current FM sensitivity of the laser. To further increase the holding range, an active filter must be used.

3.3.3 Active lag-lead filter to increase the holding range

A second-order active filter can potentially provide a current of tens of mA and thus provide a holding range of multiple GHz. It can also provide excellent low frequency noise reduction since the loop gain is significantly enhanced at low frequency. Fig. 3.16(a) is the circuit diagram of a second-order active filter with the transfer function $F(s)=(1+\tau_2 s)/\tau_1 s$. Since it is an all-pass filter for signals from DC to very high frequency, it requires a very high speed Operational amplifier(Op-Amp) with a flat phase response.

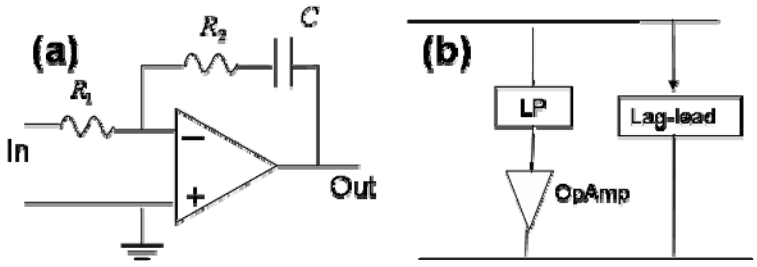

OpAmp: operational amplifier

Fig. 3.16 (a) Schematic diagram of a second-order active filter. (b) Schematic diagram of an active lag-lead filter.

I take a different approach to address the problem. Another active feedback path can be added in addition to the passive feedback path to increase the feedback current and the

loop gain at low frequency. Fig. 3.16(b) is a schematic diagram of the dual-path filter. The passive path could be the typical passive lag-lead filter I have discussed. The active path is made of a low-pass filter followed by an Op-Amp.

To analyze the total effect of this filter, one can add the transfer functions of the dual feedback paths

$$F_{tot}(s) = F_1(s) + F_2(s)A \tag{3.55}$$

where $F_1(s)$, $F_2(s)$, and A represent, respectively, the transfer function of the passive feedback path, the filter in the active feedback path, and the Op-Amp gain. For the sake of simplicity, I assume that $F_1(s) = 1$, and $F_2(s)$ is a low-pass filter described by $F_2(s) = 1/(1 + s/\omega_c)$. The gain A>>1 is a constant for frequency much lower than the bandwidth of the OpAmp. Then Eq. (3.55) becomes

$$F_{tot}(s) \approx A\frac{1 + s/A\omega_c}{1 + s/\omega_c} \tag{3.56}$$

Eq. (3.56) is essentially the transfer function of a lag-lead filter (Eq. (3.53)) except for a constant gain factor A. The advantage of this active filter design is the elimination of the need of a high speed Op-Amp. A slow and low noise Op-Amp is ideal for building this active lag-lead filter. A typical Op-Amp can easily drive 10~100mA current, which is equivalent to a holding range of multiple GHz.

An example of such an active lag-lead filter is realized and tested in an OPLL made of an external cavity laser. The schematic diagram of the circuit is given in Fig. 3.17. The OPLL has an initial holding range of around +/-50MHz. The current FM sensitivity of the laser is about 150MHz/mA. A passive lag-lead filter is first implemented to increase the holding range to ~+/-300MHz. This corresponds to ~+/-2mA current output of the RF mixer. I then add the parallel active feedback path. This filter first detects the voltage signal from a resistor in the passive lag-lead filter. The voltage signal is amplified by a differential amplifier with a gain of 40 times and filtered by a low-pass filter. A second

stage Op-Amp with adjustable gain followed by a voltage-to-current conversion circuit is then used to further amplify the signal and convert it into current feedback signal. The cutoff frequency of the low-pass filter is 8Hz. The maximum gain of this active feedback path is about 20, which in theory should increase the holding range from +/-300MHz to +/-6GHz. With this filter, I can change the laser diode bias current by +/-30mA without losing lock, which indicates the holding range is +/-4.5GHz.

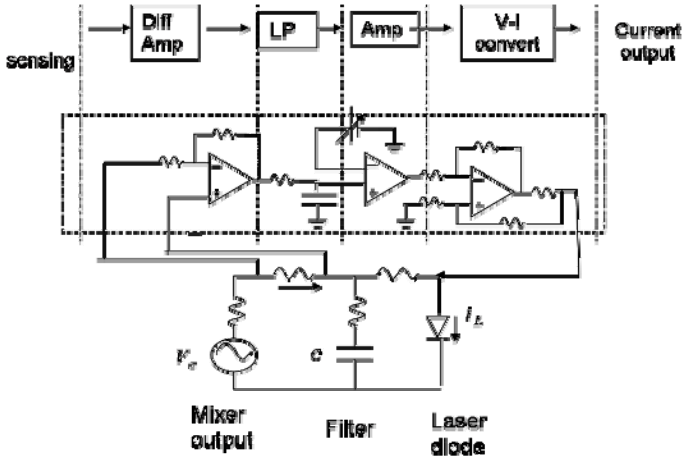

Fig. 3.17 Circuit diagram of the active lag-lead filter

If even higher holding range is desired, I can feed the current signal of the active path into the TEC controller to temperature-modulate the frequency. Due to the very high temperature FM sensitivity of SCLs, this should potentially increase the holding range by orders of magnitude. Another possible benefit of the temperature modulation is that it avoids the intensity variation caused by the feedback current modulation.

3.3.4 Aided-acquisition circuit to increase the acquisition range

So far I have discussed the use of different filters to compensate for the holding range. However the acquisition range can not be improved significantly with the lag-lead filter. To bring the laser in lock automatically upon being powered on, an aided acquisition circuit can be used. This circuit also automatically bringd the laser back to lock if the loop loses lock occasionally.

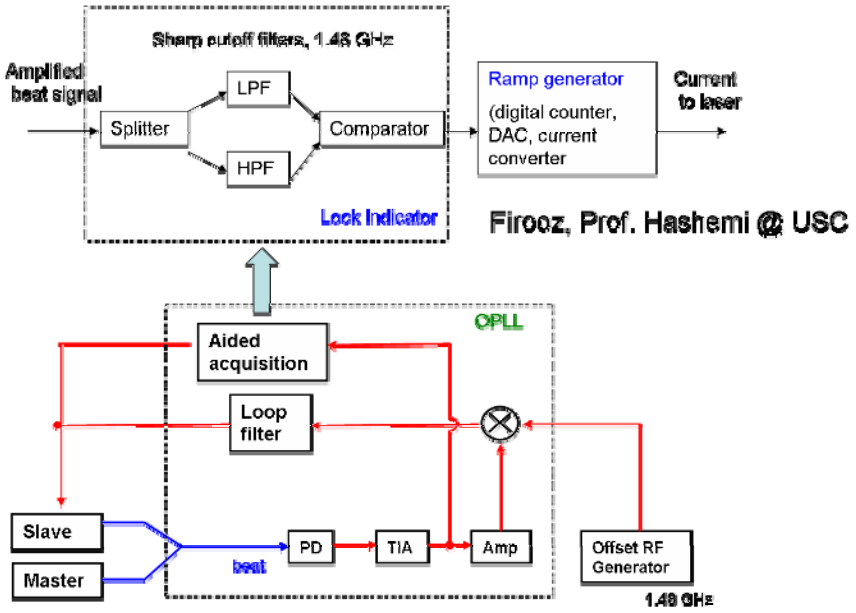

Fig. 3.18 Schematic diagram of an aided-acquisition circuit

Fig. 3.18 is a schematic diagram of an aided acquisition circuit designed and built by Firooz Aflatouni and Prof. Hossein Hashemi at USC. This circuit splits the beat signal and feeds it into a sharp low-pass filter and a high-pass filter. By comparing the output of the two filters, the circuit decides whether the frequency of the beat signal is smaller or larger than the frequency of the RF offset signal, and generates a current ramp which brings the frequency of the beat signal to be within the acquisition range of the OPLL [43]. The AAC is tested on both the QPC OPLL and the IPS OPLL. The acquisition range is increased from ±10MHz to ±1.1GHz.

3.4 Conclusion

I have successfully phase locked various commercial SCLs. The loop performance is mainly limited by the non-uniform FM response of the SCLs and the loop delay. With the use of compensation filters, the acquisition range and holding range are significantly increased. A locking efficiency of above 90% and a locking time of a few hours have been achieved. Although discrete components have been used in all the experiments demonstrated in this chapter, an integrated circuits having the function of the locking

circuits including the RF mixer, the RF amplifier, and the compensation filters can be designed and used to significantly reduce the system's dimension and cost. Research in this direction is currently being carried out by Firooz Aflatouni and Prof. Hossein Hashemi at USC.

Starting with the next chapter, I will study the applications of OPLLs, particularly in coherent beam combining and coherence cloning.